Biochimica et Biophysica Acta 1857 (2016) 1705–1714

Contents lists available at ScienceDirect

Biochimica et Biophysica Acta

journal homepage: www.elsevier.com/locate/bbabio

The obligate respiratory supercomplex from *Actinobacteria*

Wei-Chun Kao [a], Thomas Kleinschroth [a], Wolfgang Nitschke [b], Frauke Baymann [b], Yashvin Neehaul [c], Petra Hellwig [c], Sebastian Richers [d], Janet Vonck [e], Michael Bott [f], Carola Hunte [a,*]

[a] Institute of Biochemistry and Molecular Biology, ZBMZ, Faculty of Medicine, University of Freiburg, BIOSS Centre for Biological Signalling Studies, 79104 Freiburg, Germany
[b] Laboratoire de Bioénergétique et Ingénierie des Protéines UMR 7281 CNRS/Aix Marseille Univ, FR3479, 13009 Marseille, France
[c] Laboratoire de bioélectrochimie et spectroscopie, UMR 7140, Chimie de la matière complexe, CNRS-Université de Strasbourg, 1 rue Blaise Pascal, 67070 Strasbourg, France
[d] Department of Molecular Membrane Biology, Max Planck Institute of Biophysics, Max-von-Laue-Straße 3, 60438 Frankfurt am Main, Germany
[e] Department of Structural Biology, Max Planck Institute of Biophysics, Max-von-Laue-Straße 3, 60438 Frankfurt am Main, Germany
[f] Institute of Bio- and Geosciences, IBG-1: Biotechnology, Forschungszentrum Jülich, 52428 Jülich, Germany

ARTICLE INFO

Article history:
Received 25 February 2016
Received in revised form 27 June 2016
Accepted 23 July 2016
Available online 27 July 2016

Keywords:
menaquinone
Actinobacteria
respiratory chain
cytochrome oxidase
cytochrome bc_1 complex
supercomplex

ABSTRACT

Actinobacteria are closely linked to human life as industrial producers of bioactive molecules and as human pathogens. Respiratory cytochrome *bcc* complex and cytochrome aa_3 oxidase are key components of their aerobic energy metabolism. They form a supercomplex in the actinobacterial species *Corynebacterium glutamicum*. With comprehensive bioinformatics and phylogenetic analysis we show that genes for cyt *bcc-aa*$_3$ supercomplex are characteristic for *Actinobacteria* (*Actinobacteria* and *Acidimicrobiia*, except the anaerobic orders *Actinomycetales* and *Bifidobacteriales*). An obligatory supercomplex is likely, due to the lack of genes encoding alternative electron transfer partners such as mono-heme cyt *c*. Instead, subunit QcrC of *bcc* complex, here classified as short di-heme cyt *c*, will provide the exclusive electron transfer link between the complexes as in *C. glutamicum*. Purified to high homogeneity, the *C. glutamicum bcc-aa*$_3$ supercomplex contained all subunits and cofactors as analyzed by SDS-PAGE, BN-PAGE, absorption and EPR spectroscopy. Highly uniform supercomplex particles in electron microscopy analysis support a distinct structural composition. The supercomplex possesses a dimeric stoichiometry with a ratio of *a*-type, *b*-type and *c*-type hemes close to 1:1:1. Redox titrations revealed a low potential *bcc* complex ($E_m^{ISP} = +160$ mV, $E_m^{b_L} = -291$ mV, $E_m^{b_H} = -163$ mV, $E_m^{cc} = +100$ mV) fined-tuned for oxidation of menaquinol and a mixed potential aa_3 oxidase ($E_m^{CuA} = +150$ mV, $E_m^{a/a3} = +143/+317$ mV) mediating between low and high redox potential to accomplish dioxygen reduction. The generated molecular model supports a stable assembled supercomplex with defined architecture which permits energetically efficient coupling of menaquinol oxidation and dioxygen reduction in one supramolecular entity.

1. Introduction

The phylum *Actinobacteria* [1] comprises medically and economically very important species, such as industrial producers of a variety of bioactive molecules and human pathogens. Examples include *Streptomycetes*, which are the most abundant source of natural antibiotics [2], and the soil bacterium *Corynebacterium glutamicum*, which is used for production of glutamate and lysine at megaton scale per year and which has superior potential for production of other chemicals such as organic acids, diamines, or biofuels and for proteins [3,4]. Closely related to *C. glutamicum* are the diphtheria and tuberculosis (TB) causing species *C. diphtheriae* and *Mycobacterium tuberculosis* [5,6]. In aerobic respiration, which is a predominant form of cellular energy conversion in *Actinobacteria*, exergonic electron transfer through respiratory chain complexes with dioxygen as terminal acceptor generates proton motive force (PMF) that drives ATP synthesis. Respiratory complexes can associate in supramolecular associations, the so called respiratory supercomplexes. They have been intensely studied in mitochondria [7], in which they may organize electron flux for an optimal use of available substrates [8]. Little is known about the actinobacterial counterpart. An actinobacterial respiratory supercomplex was first reported for *C. glutamicum* [9,10]. In this supercomplex, electron transfer from menaquinol to dioxygen is facilitated by a sequential reaction of cytochrome *bcc* complex[1] (*bcc* complex) and cytochrome aa_3 oxidase (aa_3 oxidase) which both contribute to PMF generation [11,12]. Co-purification of the complexes demonstrated their supramolecular

Abbreviations: E_m, midpoint potential; PMF, proton motive force; SEC, size exclusion chromatography; TB, tuberculosis.

* Corresponding author.
E-mail address: carola.hunte@biochemie.uni-freiburg.de (C. Hunte).

[1] Cytochrome *bcc* complex rather than cytochrome bc_1 complex is used for a consistent nomenclature in prokaryotic and eukaryotic respiratory complexes.

http://dx.doi.org/10.1016/j.bbabio.2016.07.009
0005-2728/

association and quinol oxidase activity [13]. No additional cytochrome *c* (cyt *c*) is present for electron transfer between the two complexes in *C. glutamicum*, as staining of protein extracts from whole cells for covalently bound heme showed the presence of a single, membrane bound *c*-type cytochrome, the di-heme QcrC subunit of *bcc* complex [13]. QcrC mediates electron transfer between the two enzymes, both heme groups of the di-heme class I cytochrome *c* are essential for the transfer [13].

C. glutamicum has a second branch of the respiratory chain with lower bioenergetic efficiency, in which the *bd* quinol oxidase directly oxidizes quinol and reduces dioxygen [12,14,15]. As *C. glutamicum* lacks a proton pumping NADH dehydrogenase, the major energy transducer in oxygenic oxidative phosphorylation are *bcc* complex and aa_3 oxidase. This is confirmed by the growth defect observed for a mutant lacking the *bcc* complex [15]. This supercomplex is thus of interest for optimizing efficiency in industrial production [11] and may provide opportunities to combat drug-resistant forms of TB [16]. Interestingly, *bcc* complex from *Mycobacterium tuberculosis* and aa_3 complex from *Mycobacterium smegmatis* were recently combined in a hybrid actinobacterial supercomplex similar to that of *C. glutamicum* [17]. The underlying structural and energetic principles of this supermolecular association are not clear and the question arises whether *bcc* complex and aa_3 oxidase generally form a supercomplex in *Actinobacteria*.

In respiratory chains, exergonic electron transfer is facilitated through a series of enzyme-embedded redox centers with increasing midpoint potentials. Different potentials are also known for the small lipophilic quinone molecules which transfer electrons between enzyme complexes *via* diffusion in the membrane. These quinones are specific to organisms and are used as taxonomic markers [18]. In contrast to many other aerobic organism which use high potential ubiquinone ($E_{m7} = 90$ mV) [19], *Actinobacteria* as all other Gram-positive bacteria possess the low potential menaquinone ($E_{m7} = -74$ mV) [18,20]. A correlation of high- and low-potential respiratory chains with ubiquinone and menaquinone, respectively, has been suggested [21]. Low redox potentials were measured for the Rieske iron sulfur protein (ISP), the quinol oxidizing subunit of *bc* complexes, of some menaquinone utilizing organisms [21,22]. Furthermore, our recent sequence analysis of cyt *b* and Rieske ISP suggested that the enzyme co-evolved with the substrate quinone species [23], and we proposed a low potential for these two catalytic subunits of actinobacterial *bcc* complex. However, with dioxygen as terminal electron acceptor, high potential cofactors are expected towards the oxygen reducing end.

Here we show with bioinformatics and phylogenetic analysis that not only the *C. glutamicum* genome harbors the genes encoding the cyt *bcc*-aa_3 supercomplex but that this genetic composition is characteristic for the majority of *Actinobacteria*. The analysis also demonstrates that the phylum lacks genes for additional class I cyt *c*, which could accomplish electron transfer between *bcc* complex and aa_3 oxidase, the homologs of mitochondrial complexes III and IV. Instead, the link between menaquinol-oxidizing and oxygen reducing complex and the characteristic feature of the supercomplex is subunit QcrC, which is shown to be a short di-heme cyt *c*. We therefore term the actinobacterial *bcc*-aa_3 supercomplex an obligatory supercomplex. Purified to homogeneity, the defined dimeric stoichiometry and highly uniform particles clearly indicate a distinct structural composition of the obligate supercomplex, which was substantiated by a structural model. The redox-tuned supercomplex has a low potential *bcc* complex, as predicted on the basis of the PDWY sequence for the Q_o motif of actinobacterial cyt *b* [23], and a mixed-type potential aa_3 oxidase, thus accepting electrons with a low potential side and donating them to dioxygen with a high potential side. The stable assembled supramolecular association permits energetically efficient coupling of menaquinol oxidation and dioxygen reduction.

2. Materials and methods

2.1. Cell cultivation, membrane preparation and purification of bcc-aa_3 supercomplex

For production of supercomplex, *C. glutamicum* strain ΔC-D_{St} (13032Δ*ctaD* with pJC1-*ctaD*$_{St}$) was cultivated as described [13] in buffered medium (100 mM potassium phosphate buffer, pH 6.8). 30 g of cells was suspended in 90 ml of 100 mM Tris-HCl (pH 7.5), 5 mM $MgSO_4$ and trace amount of Benzonase (Novagen) and broken by a Constant cell disrupter (TS series) at 35 kpsi with four passages. After removal of cell debris (10,000 ×*g* for 30 min), the membranes were sedimented by ultracentrifugation (43,000 ×*g* for 15 h). 1 g of cell membrane was solubilized in 20 ml of 100 mM Tris-HCl (pH 7.5), 2 mM $MgSO_4$, 100 mM NaCl, 1% dodecyl-maltopyranoside (DDM) for 45 min at 4 °C. Insoluble material was removed by ultracentrifugation at 185,000 ×*g* for 40 min, and the supernatant was subjected to streptavidin purification using a Strep-Tactin Superflow-HR column (IBA GmbH) equilibrated with Buffer W (100 mM Tris-HCl, 2 mM $MgSO_4$, 100 mM NaCl and 0.015% DDM). Supercomplex was eluted in one step with 2.5 mM D-desthiobiotin dissolved in Buffer W and consequently purified *via* size-exclusion chromatography (TSKgel G4000 SW column, 7.5 mm × 60 cm, TOSOH Bioscience) using the same buffer without D-desthiobiotin. For calibration, the High Molecular Weight Gel Filtration Calibration Kit (GE Healthcare) was used. The purified protein was analyzed by SDS-PAGE (14% acrylamide/bisacrylamide) [24] and Blue-Native PAGE [25] and was visualized by silver staining.

2.2. Biochemical and biophysical analysis

The concentration of supercomplex was quantified from dithionite-reduced minus ferricyanide oxidized redox difference spectra at room temperature, using the respective extinction coefficients: heme *a* $\Delta_{600-630} = 11.6\ mM^{-1}\ cm^{-1}$, heme *b* $\Delta_{562-577} = 22\ mM^{-1}\ cm^{-1}$, heme *c* $\Delta_{552-540} = 19.1\ mM^{-1}\ cm^{-1}$ [13]. The redox midpoint potentials of *a*-, *b*- and *c*-type hemes were determined by electrochemical titrations using an electrochemical thin layer cell [26] and monitored by absorbance spectroscopy from 400 to 800 nm as described before [27,28]. The purified supercomplex was dissolved in 50 mM sodium phosphate buffer pH 7.0, 100 mM NaCl, 20 mM $MgSO_4$ and 0.01% DDM. 7 μl of the protein was mixed with a cocktail of mediators at a final concentration of 25 μmol/l [29] for at least 1 h before loading into the electrochemical cell. The sample was titrated from −450 to +450 mV (SHE) at 10 °C, with a potential step of either 25 or 50 mV, and an equilibration time varying from 30 to 60 min per step. The absorbance spectra were recorded with a Cary 300 spectrophotometer. 5 spectra were averaged to improve the signal to noise ratio.

The redox midpoint potential of Rieske iron-sulfur cluster and Cu_A was determined by redox titration and monitored by EPR spectroscopy. EPR spectra were recorded on a Bruker Elexsys E500 X-band spectrophotometer fitted with an Oxford Instruments He-cryostat and temperature control system. Conditions are indicated in the figure legend. Redox titrations were performed as described [30] in the presence of 50 mM MOPS buffer pH 7, 2 mM KCN, 20 mM glucose, glucose oxidase and mediators *p*-benzoquinone, 2,5-$(OH)_2$ *p*-benzoquinone, 1,2-naphtoquinone, phenazine methyl sulfate, and methylene blue at 100 μM each. Reductive titrations were carried out by sodium dithionite, oxidative titrations by ferricyanide. The amount of reduced Rieske iron-sulfur cluster was evaluated on the g_y line. EPR settings: temperature 15 K, microwave power 6.4 mW, microwave frequency 9.48 GHz, modulation amplitude 0.003 mT. The binding of stigmatellin was measured with EPR spectroscopy using streptavidin affinity chromatography purified supercomplex (38 μM) and following EPR settings: temperature 15 K, microwave power 6.4 mW, microwave frequency 9.48 GHz, modulation amplitude 0.001 mT.

2.3. Electron microscopy and single particle analysis

The supercomplex samples were prepared on glow-discharged carbon-coated copper grids and negatively stained with 1% (w/v) uranyl acetate. Electron micrographs were taken on a Philips CM120 microscope at 120 kV under low dose conditions at a 44,000 fold magnification on Kodak SO-163 electron image film. The negatives were analyzed by optical diffraction for correct defocus, lack of drift and astigmatism and digitalized by a PhotoScan scanner at a pixel size of 7 μm, corresponding to 1.59 Å on the specimen. Subsequently adjacent pixels were averaged to yield a pixel size of 4.77 Å. Total 1600 particles were selected and subjected to multi-reference alignment, multivariate statistical analysis and classification using the IMAGIC-5 image processing package [31].

2.4. Bioinformatic analysis

Cyt *c* protein sequences were identified using HMMER (v. 3) [32] with the profile hidden Markov model of class I cyt *c* (PF00034 from the Pfam database, [33]) against the non-redundant, curated NCBI Reference Sequence (RefSeq) protein database release 59 (May 2013) [34]. All the protein sequences above the default inclusion threshold (e-value lower than 1e-3) were collected. In addition, HMMER counts the number of cyt *c* domains, which facilitates the classification of multiple-domain proteins. The number of di-heme cyt *c* was reduced by homology clustering using the CD-HIT application [35] with threshold set to 40% identities, and 640 sequence representatives were selected. To define di-heme cyt *c* as a subunit of *bcc* complex (QcrC), it is presumed that *qcrC* should be allocated with cyt *b* (*qcrB*) and Rieske ISP (*qcrA*) in the *qcrABC* gene cluster, or the homologous *petABCD* cluster in the same genome. QcrB sequences were fetched by the profile hidden Markov model of cytochrome *b* N-terminal domain (PF00032) from the RefSeq database. The locus_tag associated with each sequence was analyzed for all di-heme cyt *c* and QcrB [23]. 21 di-heme cyt *c* were found in the same gene cluster with cyt *b*, and therefore these sequences were defined as di-heme QcrC. For phylogenetic analysis, the di-heme QcrC of *C. glutamicum* was used to replace the di-heme QcrC from *Corynebacterium pseudotuberculosis* (YP_006213938). CLUSTAL Omega [36] was used for calculating sequence alignment. Bayesian phylogenetic analysis was performed with MRBayes [37] with 8 chains, 100,000 generations, burnin set to 25% of the sample, and temperature set to 0.1. Phylogenetic trees were plotted by FigTree (http://tree.bio.ed.ac.uk/software/figtree/). The standalone NCBI BLAST+ application (v. 2.28) was used for managing the local copy of RefSeq database and performing homology search [38]. Transmembrane helices were predicted by TOPCONS [39] and TMHMM [40].

Homology modeling of QcrC and construction of a model of the supercomplex catalytic core. The homology model of the soluble domain of *C. glutamicum* QcrC was obtained using the X-ray structure of CcoP from *Pseudomonas stutzeri* (PDB 3mk7, [41]) as template. Sequence alignment (CLUSTAL Omega [36]) of QcrC and CcoP was optimized for gap position. The sequences have 49% similarity (Table S1, Fig. S1). The program MODELLER was used for modeling (http://salilab.org/modeller; [42]). The model of the catalytic core of the supercomplex was constructed by manual docking of X-ray structures of homologous complexes and the QcrC homology model. QcrC was superimposed on subunit cyt c_1 of the cyt bc_1 complex from *Paracoccus denitrificans* (PDB 2yiu, [43]) and cyt c_1 was removed. The predicted transmembrane helices of Rieske ISP and di-heme QcrC were omitted (Table S1). Whereas the corresponding proteobacterial subunits have a single transmembrane helix (TMH), the former possesses three and the latter two TMHs. *C. glutamicum* QcrB has a C-terminal domain of 82 amino acids which would extend to the electronegative membrane side. Two molecules of aa_3 oxidase were positioned at each side of the *bcc* dimer using the X-ray structure of aa_3 oxidase from *Rhodobacter sphaeroides* (PDB 1m56, [44]) (Table S1). The TMH of QrcB and CtaE/F were located adjacent to each other bringing the second heme *c* and Cu_A close to a distance of 14 Å. *C. glutamicum* aa_3 oxidase would have one more TMH based on topology prediction (Table S1). The model has a two-fold symmetry.

3. Results and discussion

3.1. Genes encoding the catalytic subunits of cyt bcc-aa_3 supercomplex are characteristic for Actinobacteria

The catalytic core of the *C. glutamicum bcc-*aa_3 supercomplex consist of subunits QcrA, QcrB, QcrC, CtaC, CtaD, CtaE and CtaF, which are encoded by the gene clusters *qcrABC* and *ctaCEF* and gene *ctaD* (Fig. 1A and Table S1) [11]. In order to evaluate the distribution of these genes in the entire phylum *Actinobacteria*, homologous sequences were retrieved from the 732 actinobacterial genomes present in the NCBI database using HMMER homology-searching methods (see Materials and methods). Genes for the catalytic subunits are universally present in nearly all orders of the class *Actinobacteria* with the exceptions of the anaerobic orders *Actinomycetales* and *Bifidobacteriales*. They are also characteristic for the class *Acidimicrobiia* (Figs. 1B and S2).

3.2. Actinobacteria harbor di-heme QcrC genes but lack additional genes encoding c-type heme proteins

Di-heme QcrC was identified as sole *c*-type cytochrome in *C. glutamicum* and its structural and functional role for this supercomplex was shown [13]. In order to probe the exclusive presence of di-heme QcrC genes not only in *C. glutamicum* but in all phyla, a systematic analysis of the distribution of genes that encode class I cyt *c* proteins was carried out. The NCBI RefSeq protein database (Release 59, May 2013) was searched by the profile hidden Markov model of class I cyt *c* (Pfam entry PF00034). Genes encoding one up to six class I cyt *c* domains are widely distributed in the 16S rRNA based phylogenetic tree of all organisms (Fig. S3). Notably, *Actinobacteria* is the only phylum, in which genes for di-heme cyt *c* rather than mono-heme cyt *c* are predominantly present. Furthermore, genes encoding more than two cyt *c* domains are lacking in that phylum. The majority of actinobacterial di-heme cyt *c* genes belong to the *qcrABC* gene cluster and are thus di-heme *qcrC*. Most of them encode QcrC with two transmembrane helices and others with one helix (Dataset S1). They belong to the class *Actinobacteria* (513 sequences) and to the class *Acidimicrobiia* (2 sequences). The few actinobacterial genes encoding single class I cyt *c* domain proteins (11 sequences) are from the classes *Acidimicrobiia* and *Rubrobacteria*, which lack the *qcrABC* cluster (Table S2). They are fused with genes of other respiratory complexes as for instance genes of the caa_3 oxidase (Table S2) and are thus not relevant for the supercomplex. Finally, genes for copper based electron carriers such as plastocyanin were not identified in the phylum *Actinobacteria* (data not shown). To summarize, the phylogenetic analysis shows that not only *C. glutamicum* but in general *Actinobacteria* lack genes for mono-heme cyt *c* or other *c*-type heme proteins other than qcrC, strongly suggesting that di-heme QcrC is the sole link between *bcc* complex and aa_3 oxidase in an operational actinobacterial supercomplex.

3.3. Actinobacterial qcrC encode small di-heme cyt c

In order to identify specific structural features of actinobacterial di-heme QcrC, a systematic analysis of all di-heme cyt *c* protein sequences throughout all kingdoms of life was performed. All di-heme cyt *c* sequences were retrieved from the NCBI RefSeq protein database and the total of 8839 hits was reduced to 640 representatives, which share sequence identity not higher than 40% using the sequence clustering algorithm CD-HIT [35]. For the identification of di-heme cyt *c* as QcrC subunit of cyt *bc* complex, the locus tags were paired with those of

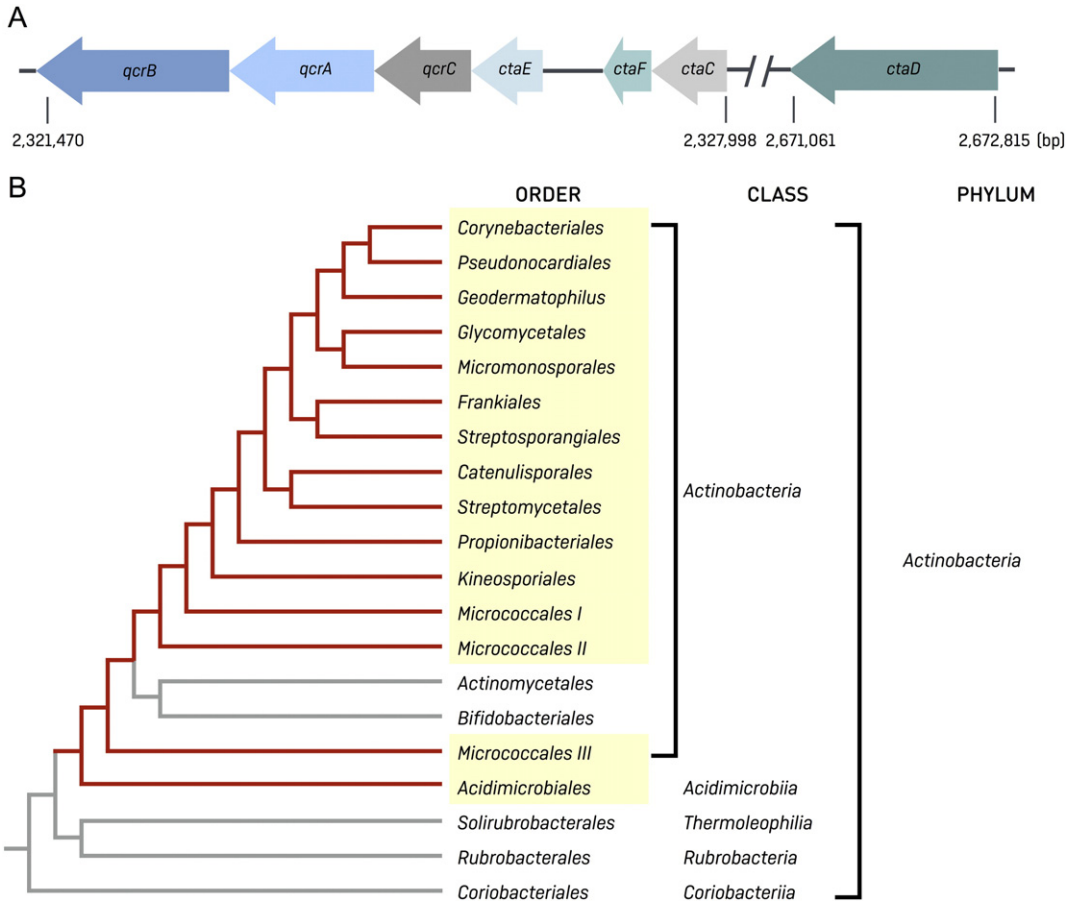

Fig. 1. Phylogenetic distribution of cyt *bcc* complex and aa_3 oxidase genes in *Actinobacteria*. (A) Schematic depiction of genes encoding cyt *bcc* complex (*qcrABC*) and aa_3 oxidase (*ctaCDEF*) according to the genome of *C. glutamicum* (http://www.ncbi.nlm.nih.gov/genome/469?genome_assembly_id=166859). *ctaD* is located 345 kb upstream of *ctaC*. (B) The occurrence of cyt *bcc* complex and aa_3 oxidase in the orders of *Actinobacteria* is mapped on a phylogenetic tree. The latter is based on the sequence of 35 conserved proteins [1] and was plotted with identical branching length. The presence of both complexes is indicated by red lines and yellow background. With the exceptions of the anaerobic orders *Actinomycetales* and *Bifidobacteriales*, the complexes are present in all other orders of the class *Actinobacteria* and in the class *Acidimicrobiia*. *Geodermatophilus* is a genus from *Frankiales*, which does not cluster with the order. *Micrococcales* is split in three branches on the tree and therefore denoted as I, II and III. Detailed statistics of the number of species encoding each enzyme subunit is summarized in Fig. S2.

QcrB [23]. In the representative di-heme cyt *c* data set, 21 QcrC sequences were identified. Remarkably, they show a systematic difference in length and were categorized accordingly into two groups (Fig.2 and Table S4). Short di-heme QcrC sequences have a length of 79–80 residues for each domain and a distance of about 37 residues between the axial heme ligands. Long di-heme QcrC sequences have an average length of 102 residues for each domain and a distance of about 62 residues between the axial ligands (Fig. 2). The classes *Actinobacteria* and *Acidimicrobiia* have short di-heme QcrC sequences (Table S4), whereas the long are found in ε-*Proteobacteria*, *Chloroflexi*, and low branching

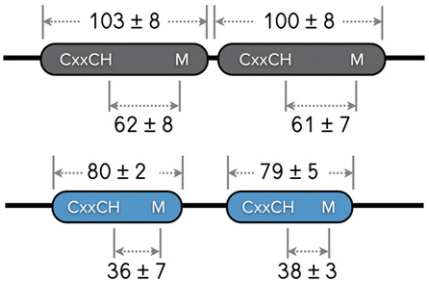

Fig. 2. Domain composition of di-heme QcrC. Domain structure of long (upper panel) and short (lower panel) di-heme QcrC. The average domain length and distances between heme axial ligand (His-Met) are listed as number of residues. They are derived from the representative data set of di-heme QcrC (see Fig. S4 and Table S4).

Firmicutes. Our classification of long and short di-heme cyt *c* sequences is consistent with Richard Dickerson's initial description of large and small soluble class I cyt *c* [45,46], *i.e.* the short di-heme QcrC comprises two small class I cyt *c* domains.

Taken together, genes of the catalytic subunits of cyt *bcc* complex and cyt aa_3 oxidase are present in nearly all orders of the phylum *Actinobacteria*. Genes of mono-heme cyt *c* are generally lacking in *Actinobacteria*. We suggest that characteristic for *Actinobacteria* is an obligate *bcc*-aa_3 supercomplex, in which direct interaction of the complexes is required to couple menaquinol oxidation and dioxygen reduction. In order to challenge this hypothesis, we analyzed the structural and energetic prerequisites of the supramolecular association using the supercomplex from *C. glutamicum* as prototype.

3.4. The stoichiometry of *bcc*-aa_3 supercomplex from *C. glutamicum*

To determine the stoichiometry within the supramolecular association, the *bcc*-aa_3 supercomplex from *C. glutamicum* was purified to high homogeneity. Streptavidin-affinity chromatography (SAC) resulted in an average yield of 0.7 mg per liter of culture. The supercomplex was stable in subsequent size-exclusion chromatography (SEC), in which symmetrical protein- and heme-specific elution profiles indicated a homogenous and mono-disperse protein preparation with an apparent molecular mass higher than 669 kDa (Fig. 3A). In Blue Native (BN) PAGE analysis, the major supercomplex fraction migrated with an apparent mass of about 1100 kDa (Fig. 3B). The SEC purified supercomplex

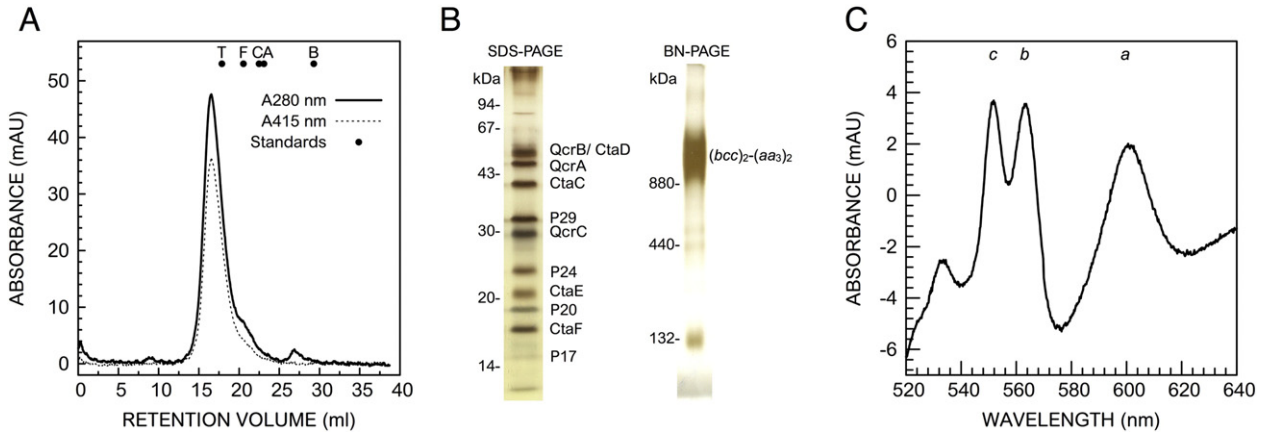

Fig. 3. Characterization of SEC-purified *bcc-aa*$_3$ supercomplex from *C. glutamicum*. (A) Elution profile of supercomplex separated on a TSKgel 4000 SW column. Retention volumes of molecular mass standard proteins are indicated with black dots: T, thyroglobulin (669 kDa); F, ferritin (440 kDa); C, catalase (232 kDa); A, aldolase (158 kDa); B, conalbumin (75 kDa). The void volume of the SEC column is 8 ml. (B) Silver-stained gel after separation of purified supercomplex by SDS- and BN-PAGE. Molecular masses of co-migrated standard proteins are indicated. Subunits with molecular masses are listed in Table S1. (C) Dithionite-reduced minus ferricyanide-oxidized absorbance spectrum of purified supercomplex. The labels *c*, *b*, and *a* indicate the absorption maxima of the respective heme types (551, 563, and 600 nm).

has a defined molecular shape. Single particle electron microscopy analysis of negatively stained specimens revealed highly homogeneous particles (Fig. 4A). Classification and averaging of 1600 images yielded two classes of particles (Fig. 4B and C). Both had a length of 22 nm, one with a width of 9 nm and the other of 10 nm. In the projection maps, they share a common central dark spot which connects to the upper boundary, and two dark three-leaf clover like structures at each side. The two classes are likely to represent the supercomplex residing on the carbon grid in two different tilting angles along its long axis. The dimensions of the particle and the lack of a clear detergent belt around it [47] suggests that the supercomplex is viewed almost perpendicular to the membrane plane, while the lack of two-fold symmetry indicates a slight tilt. SDS-PAGE analysis revealed the presence of all catalytic subunits of *bcc* complex (QcrA, QcrB, QcrC) and *aa*$_3$ oxidase (CtaC, CtaD, CtaE, CtaF) as well as of four accessory subunits previously identified (Fig. 3B) [13]. Analyzed by optical spectroscopy, the SEC purified supercomplex showed a characteristic redox difference spectrum with maximum absorbance of heme *a*, *b*, and *c* at 600, 563, and 551 nm, respectively (Fig. 3C). A molar ratio of 0.9:1.0:0.9 for *a*-, *b*-, and *c*-type hemes was determined.

The redox-active centers, namely hemes, FeS-cluster and Cu_A-center, were characterized by EPR spectroscopy (Fig. 5A). The spectral properties of all hemes are similar to those of typical cyt *bc*$_1$ and heme-copper oxidases [48], so that the $g_z = 3.65$, 3.44 and 3.35 lines could be assigned to ferric heme b_L, heme b_H, and *c*-type hemes, respectively. The low spin heme *a* was assigned to $g_x = 1.45$ and $g_z = 2.98$. An identification of Cu_A and of heme g_y-lines was hampered by the intense EPR signals between $g = 1.8$ and $g = 2.3$ (or 270 and 400 mT), owing to a characteristic manganese (Mn) incorporation into *aa*$_3$ oxidase [49]. Therefore, the supercomplex was purified from cells cultivated in medium with 400-fold lower (90 nM $MnSO_4$) concentration. The Mn^{2+} EPR signal was successfully decreased to non-detectable levels in the isolated supercomplex, and the typical signal of Cu_A became visible. In addition, a derivative-shaped line at 2.25 was clearly discernible in the Mn-depleted sample. Applying the rule for low-spin heme compounds of $\Sigma g^2 = 16$, this line could be unambiguously attributed to g_y of heme *a*.

The EPR spectrum of the dithionite reduced isolated supercomplex revealed the characteristic signal of the Rieske iron-sulfur cluster at $g_x = 1.83$ and $g_y = 1.89$ (Fig. 5B). Interestingly, the g_x value was located at 4.5 mT lower field as compared to the respective line of the bovine [50] or the *Heliobacterium chlorum* [51] enzymes. Addition of the Q_o site inhibitor stigmatellin to the isolated supercomplex resulted in a shift of this g_x signal towards higher fields from $g_x = 1.83$ to $g_x = 1.81$, accompanied by a broadening of the line. This observation is consistent with the spectral shift observed in bovine cyt *bc*$_1$ complex [50] and chloroplast cyt *b*$_6$*f* complex [52], suggesting that stigmatellin binds to the Q_o site of *C. glutamicum bcc* complex.

To summarize, the highly purified *C. glutamicum* supercomplex contained all known subunits and cofactors of *bcc* complex and *aa*$_3$ oxidase. Cyt *bc* complexes are functional dimers owing to the intertwined Rieske ISP [53], whereas *aa*$_3$ oxidases exists as dimer in mitochondria [54] or as monomer in bacteria [44]. As the purified supercomplex has an equal molar ratio of *a*-, *b*- and *c*-type hemes and dimeric *bcc* complex

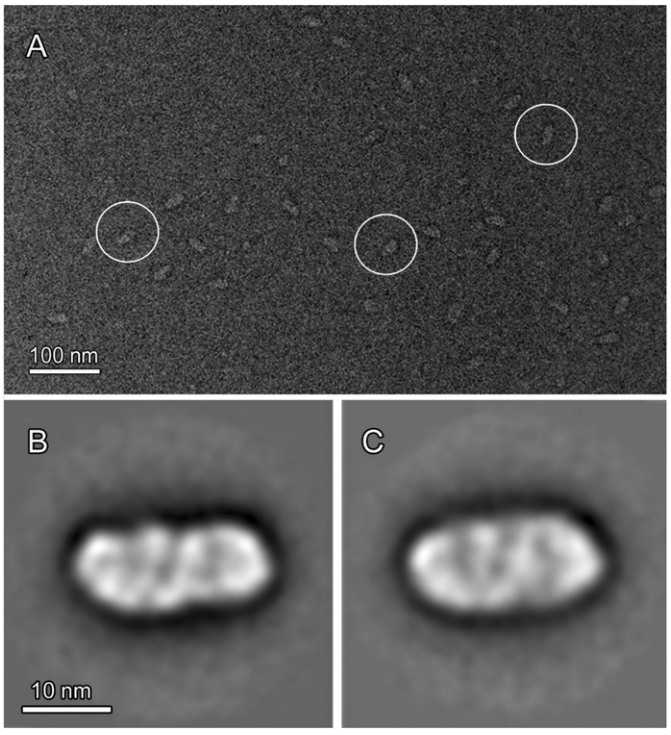

Fig. 4. Single particle negative stain electron microscopy analysis of the supercomplex. (A) Section of an electron micrograph of SEC-purified supercomplex. White circles indicate three representative particles; (B) and (C): Projection maps represent class sums of 800 aligned projections each of the supercomplex with different orientations on the supporting carbon film.

contains four *b*-type (2 heme b_L, 2 heme b_H) and four *c*-type hemes, the supercomplex thus comprises two aa_3 oxidase molecules (2 heme *a* and 2 heme a_3). Dimeric *bcc* complex with two aa_3 oxidase molecules and the minimal number of accessory subunits has a calculated mass of 605 kDa (Table S1), thus a higher oligomeric association can be excluded from SEC and BN-PAGE results. With at least 72 transmembrane helices (TMH) (Table S1) the detergent contribution to the apparent mass will be higher than the 220–230 kDa DDM micelle of dimeric ion transporters with 24 TMH [55]. For BN-PAGE, a factor of 1.8 is typically considered to correct for bound detergent, lipid and dye molecules [55,56]. Taking into account composition, apparent masses and quantification by BN-PAGE, SEC and spectroscopy, the purified *C. glutamicum* supercomplex has a dimeric $(bcc)_2$-$(aa_3)_2$ stoichiometry.

3.5. Redox-tuned cofactors of the supercomplex

As *C. glutamicum* exclusively uses menaquinone ($E_{m7} = -74$ mV) [20] rather than ubiquinone ($E_{m7} = +90$ mV) [19], the question arose how the supercomplex is redox-tuned to use a low potential substrate and oxygen as terminal electron acceptor. The midpoint potentials of the redox-active metal centers were determined for purified supercomplex by electrochemical and chemical titrations monitoring hemes by absorption spectroscopy, Rieske ISC and Cu_A by EPR spectrophotometry (Fig. 5C). The midpoint potentials of the *b*-type hemes were clearly resolved in the electrochemically induced difference spectra monitored during redox titration. The E_{m7} of heme b_H, heme b_L and Rieske ISC were determined as -163 ± 5 mV, -291 ± 5 mV and $+160 \pm 20$ mV *versus* standard hydrogen electrode (SHE′). Thus, the redox potentials of *bcc* complex are about 280 to 110 mV lower as compared to mitochondrial cyt bc_1 complex ($Em^{heme\ b_H} = +116$ mV, $Em^{heme\ b_L} = -4$ mV, $Em^{Rieske\ ISC} = +270$ mV for yeast [53]). The E_{m7} of Rieske ISC is close to the value determined for the Firmicutes menaquinol users *Heliobacterium chlorum* (120 ± 10 mV [51]) and *Bacillus* PS3 (160 ± 10 mV [57]). In line with energy conversion through the Mitchellian Q cycle, the menaquinol potential is positioned about halfway between those of Rieske ISC and heme b_L. The two-electron reductant menaquinol has to be oxidized at the Q_o site in a bifurcated manner with electron transfer to heme b_L and Rieske ISP. *C. glutamicum bcc* complex is redox-tuned to use low potential menaquinol as substrate. Furthermore, the data provide the first experimental evidence for a low potential Rieske ISC in *Actinobacteria*, which was predicted on the basis of the sequence PDWY as Q_o motif in actinobacterial cyt *b* [23] and on the sequence signature motif of the Rieske ISC environment [58]. The experimental data augment the correlation among redox potentials, quinone species and phylum-specific pattern of Q_o motif, on which the proposed molecular evolution of the quinol oxidation motif is based [23].

Rieske ISC is the conceptual electron donor for the two *c*-type hemes of QcrC. The redox transitions of the di-heme are very close and a single value at $E_{m7} = 100 \pm 20$ mV was determined. This potential is more than 160 mV lower than that of heme c_1 from the ubiquinol oxidizing α-proteobacterium *Paracoccus denitrificans* (268–338 mV [59]) and closer to that of the menaquinol oxidizing Firmicutes species *Heliobacterium modesticaldum* (71 mV [60]). In ubiquinone based respiratory chains, cyt c_1 and mobile cyt *c* have midpoint potentials around 250 mV [61,62]. The midpoint potentials of heme b_H, b_L, c_1 and Rieske ISC in *C. glutamicum* are 279, 287, 150 and 110 mV lower than the respective mitochondrial values (Fig. 6). Thus, the entire *bcc* complex is a low potential complex.

The aa_3 oxidase possesses four redox-active centers. Cu_A accepts the electron from QcrC and transfer continues through heme *a* to the binuclear center heme a_3/Cu_B. The E_{m7} of Cu_A was determined to be 150 mV, however, due to the intense Mn EPR signal around $g = 2$, the error was estimated as 50 mV. It is considerably lower as compared to the mitochondrial center (290 mV, [62]), thus, the entry point to the oxidase is of low potential. Hysteresis was observed for titration of *a*-type hemes (Fig. S5). It results from anti-cooperative interaction between all oxidase cofactors, which is crucial for enabling and regulating the function of the enzyme and midpoint potentials of heme *a* and a_3 cannot be individually assigned [63]. The average of the lower heme a/a_3 potential ($Em^{a/a3(1)} = +143$ mV) is about 80 mV lower than that of mitochondrial cyt *c* oxidase (220 mV [63]), thus it is close to the potentials of di-heme QcrC and Cu_A in line with a lower potential chain. In contrast, the higher heme a/a_3 potential ($Em^{a/a3(2)} = +317$ mV) is only slightly below the mitochondrial value ($E_m = +360$ mV [63]). This appears to be reasonable as dioxygen is the common substrate. The aa_3 oxidase thus connects low and high potential cofactors in one complex, and can be considered a mixed potential complex.

Taken together, low potential *bcc* complex provides the largest contribution to accommodate the 170 mV potential difference between menaquinone and ubiquinone. The differences between redox potentials of *C. glutamicum* and mitochondrial cyt bc_1 complex and cyt *c* oxidase are largest for the *b*-type hemes and have medium values for Rieske ISC, *c*-type hemes and Cu_A (Fig. 6). For the *a*-type hemes, the difference alleviates from 80 mV to 40 mV. The electron transfer machinery of the actinobacterial supercomplex is elaborately fine-tuned for menaquinol oxidation and dioxygen as electron acceptor. Structural characterization is required to resolve how individual cofactor environment and overall structural composition facilitates the integrated supercomplex activity.

3.6. A structural model of the supercomplex compliant with biological electron transfer

A close contact between *bcc* complex and aa_3 oxidase is needed for a functionally assembled supercomplex, as biological electron transfer requires distances of 14 Å or less for donor and acceptor cofactors [64]. As QcrC is the electron bridge from Rieske ISP to the oxidase, it appears plausible that the supercomplex has a defined architecture which is structurally constrained by QcrC. Using the NCBI conserved domain database [65], a CcoP-protein domain (PF13442) was identified in *C. glutamicum* QcrC. CcoP is the di-heme cyt *c* subunit of cbb_3 oxidase. It is very similar in domain length and axial heme ligands spacing (Table S4) compared to *C. glutamicum* QcrC (Fig. S1). A homology model of the latter was constructed using the X-ray structure of CcoP from *Pseudomonas stutzeri* [41] as template. Notably, the heme ligation is shared between the two domains in CcoP owing to interdomain helix swapping [41]. Indeed, a homology model was readily constructed keeping the conformation of interdomain helix swapping as in CcoP (Fig. 7). The two hemes are facing each other with their propionate groups in 3-Å distance, the vinyl and methyl groups of the hemes protrude in crevices to the protein surface. It is tempting to speculate that all actinobacterial short di-heme QcrC have intertwined domains.

A structural model of *C. glutamicum* supercomplex could now be constructed using the QcrC homology model and X-ray structures of homologous cyt bc_1 complex from *Paracoccus denitrificans* [43] and aa_3 oxidase from *Rhodobacter sphaeroides* [44] (Fig. 8, Table S1). As the supercomplex has a dimeric $(bcc)_2$-$(aa_3)_2$ stoichiometry and cyt *b* and Rieske ISP comprise an inseparable functional dimeric core, each of its monomers has to interact with an aa_3 oxidase molecule through subunit QcrC. For construction of the model, subunit cyt c_1 of cyt bc_1 complex was replaced with di-heme QcrC superimposing the carboxyl-terminal *c*-type heme of di-heme QcrC onto heme c_1. The heme crevice faces the Rieske ISP with a cofactor distance close to 14 Å. The structure of aa_3 oxidase was subsequently positioned adjacent to it, aligning Cu_A to the amino-terminal heme crevice of QcrC and keeping the cofactor distance close to 14 Å. The model has a compact rectangular shape with dimensions of 180 Å × 90 Å × 40 Å. The cofactor containing extramembranous domains including those of di-heme QcrC form an even layer on top of the transmembrane subunits. The model has a two-fold symmetry and fulfills distance constraints and dimeric

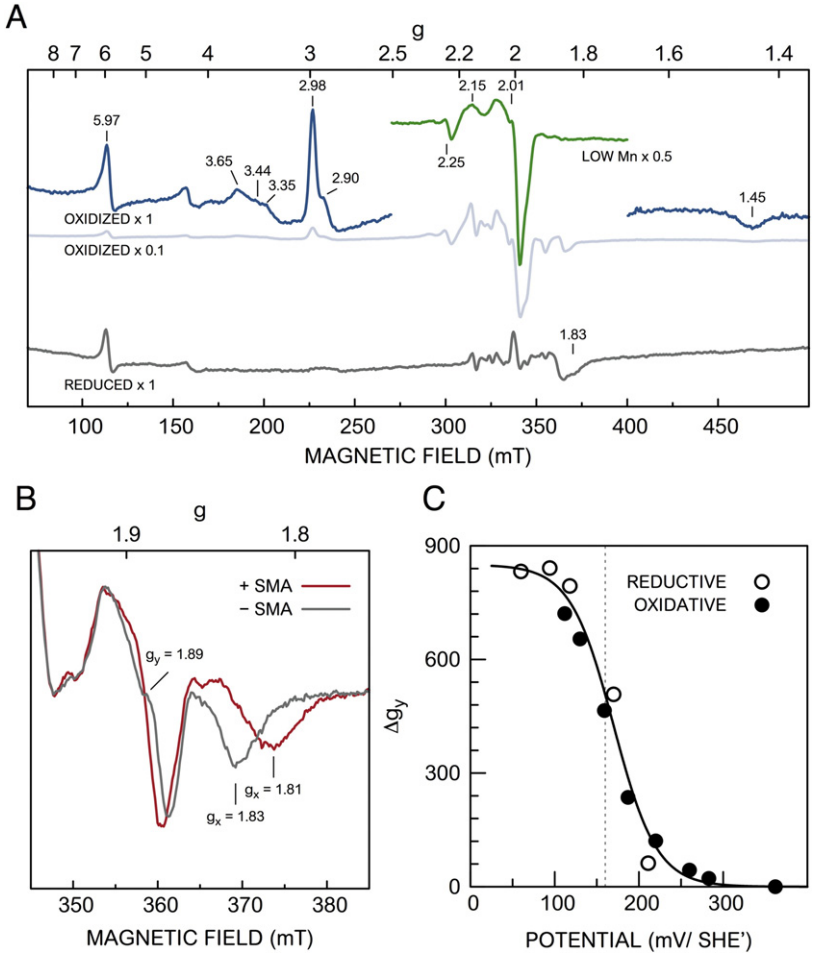

Fig. 5. Biophysical characterization of purified supercomplex by EPR spectroscopy. (A) EPR spectra of oxidized and reduced supercomplex. An intense Mn signal is visible between 300 and 350 mT (scaled to 0.1×, oxidized). EPR signals of low-spin hemes ($g = 3.65, 3.44, 3.35, 2.98, 2.90$ and 1.45) are present. EPR signal from the Cu_A site ($g = 2.01, 2.15, 2.23$) was measured from the supercomplex purified from a culture with 90 nM Mn^{2+}. The Rieske g_x signal (1.83) is present in the reduced sample. (B) Binding of 20 μM stigmatellin (SMA) shifted the g_x signal of the reduced Rieske iron-sulfur cluster (ISC) from 1.83 to 1.81. (C) The midpoint potential of Rieske ISC was determined at 160 mV (SHE′) by fitting the amplitude of the g_y line to a $n = 1$ Nernst curve. The amount of reduced Rieske ISC was evaluated on the g_y line.

stoichiometry of the catalytic core. This architecture would permit integrated menaquinol oxidase activity catalyzed by the supercomplex without the addition of extra diffusible electron carriers. Notably, electron transfer between the two heme *c* cofactors would take place close and parallel to the membrane, whereas in the mitochondrial membrane, electrons are transferred between cyt c_1 and cyt *c* at least 35 Å above and perpendicular to the membrane.

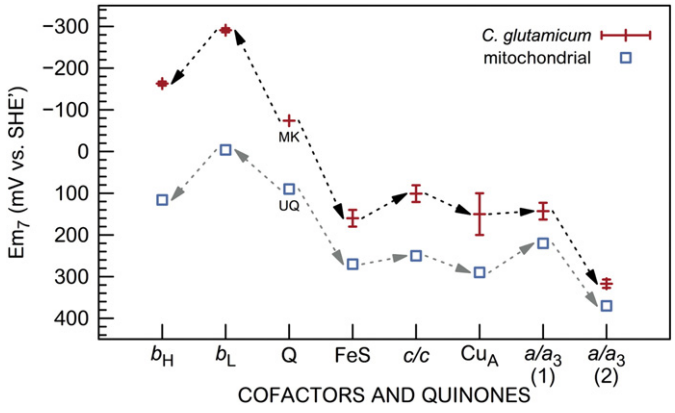

Fig. 6. Midpoint potentials determined for the purified supercomplex are shown in red with estimated errors. For comparison, midpoint potentials of mitochondrial enzymes as well as of the averaged two-step midpoint potential of the quinone substrate (Q) of *C. glutamicum* (menaquinol/-quinone, MK) and mitochondria (ubiquinol/-quinone, UQ) are shown (see text for references). The electron transfer routes between the cofactors are indicated with arrows, starting with ubi(mena)quinol oxidation at the Q_o site and bifurcated electron transfer towards FeS and heme b_L.

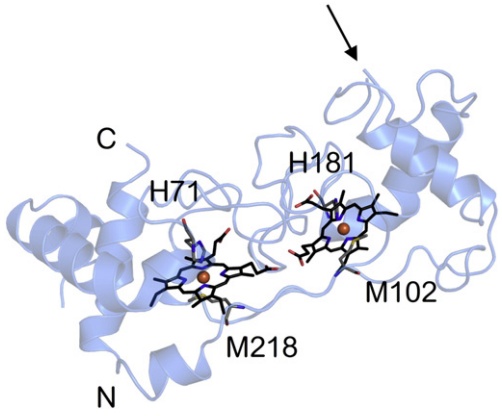

Fig. 7. Homology model of soluble domain of *C. glutamicum* QcrC using the X-ray structure of CcoP as template. The short di-heme cyt *c* has an intertwined heme coordination and axial heme ligands are indicated. C and N indicate the terminal TMH positions. The insertion 134–149 was omitted (arrow).

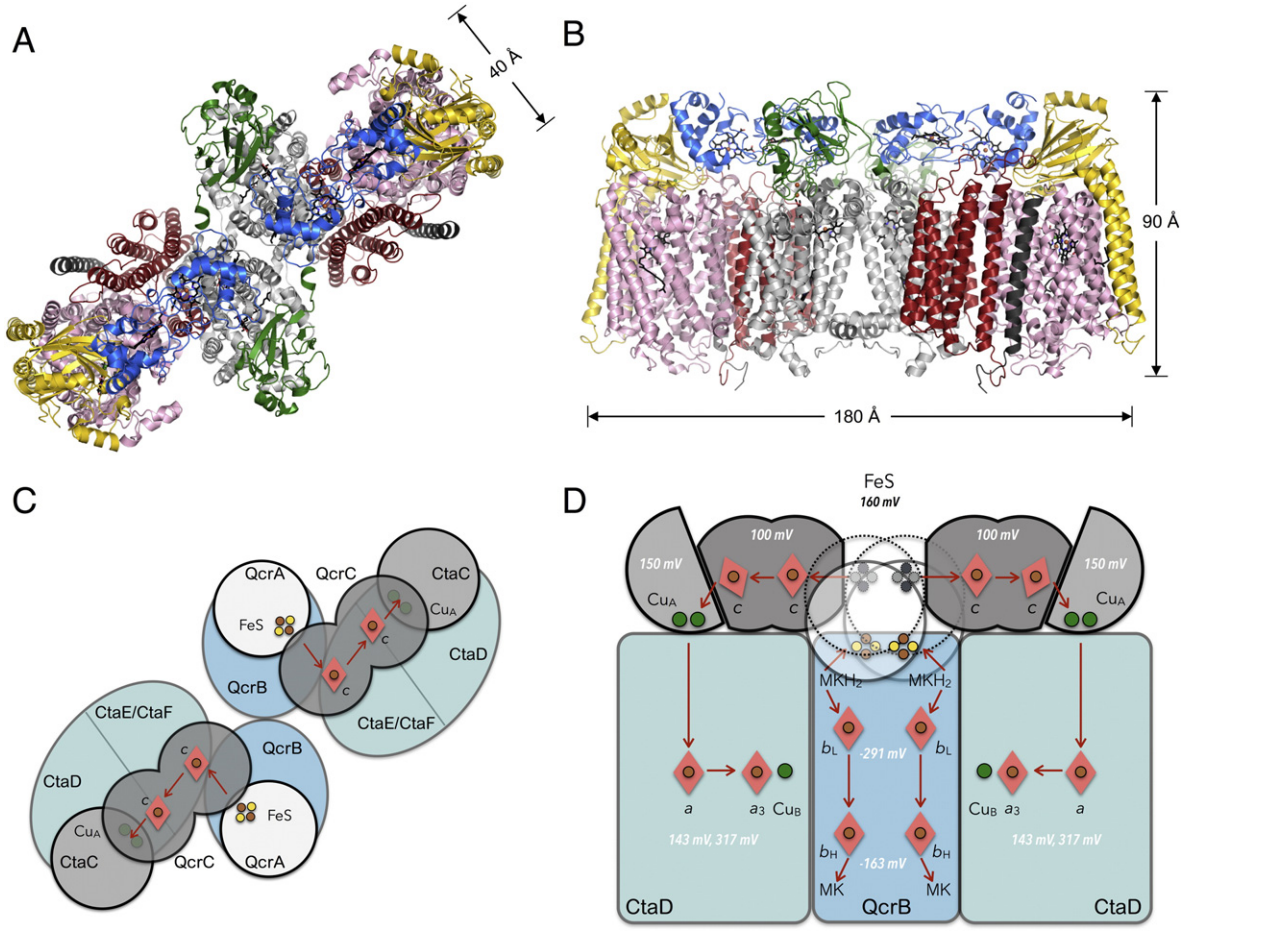

Fig. 8. Structural model of *C. glutamicum* respiratory chain supercomplex based on the biochemical and biophysical characterization of its compositions. (A) The structural model of the catalytic core supercomplex was built based on X-ray structures of QcrB (gray) and QcrA (Rieske ISP, green) from *P. denitrificans* (pdb 2yiu), X-ray structures of CtaD (pink), CtaC (yellow), CtaE (red) and CtaF (black) from *R. sphaeroides* (pdb 1m56), and the homology model of *C. glutamicum* QcrC (blue) viewed perpendicular to the membrane and parallel from the electro-positive side of the membrane (B). (C) Schematic representation of the subunit arrangement of the catalytic core of *bcc-aa*$_3$ supercomplex model viewed perpendicular to the membrane and parallel to the membrane (D), with the values of midpoint potential of redox active centers determined in this study. The electron transfer direction is indicated in red.

3.7. Supramolecular association with fine-tuned redox potentials permits efficient energy conservation

In respiratory chains, the free energy released from the stepwise exergonic electron transfer is conserved through proton translocation across the membrane. Dynamics and stoichiometry of respiratory chain components are of functional importance. Whereas information on bacterial respiratory supercomplexes is scarce, mitochondrial supercomplexes have been intensely studied. In mitochondria, which are highly dynamic organelles, there appears to be a dynamic distribution between freely diffusing complexes and supramolecular associations depending on the cellular conditions [8,66]. Our data strongly suggests that actinobacterial *bcc-aa*$_3$ supercomplex operates a structural entity with a defined architecture. For mitochondria, the generated PMF results in an energy cost of 200 meV for one positive charge transferred [62]. Thus an oxidizing cyt *c* pool or a reducing ubiquinol pool is required to drive mitochondrial cyt *bc*$_1$ complex activity under physiological conditions, as the reduction of cyt *c* by ubiquinol gives a free energy difference of 160 meV under standard conditions. In *C. glutamicum*, an *in vivo* PMF of 200 mV was experimentally determined [67], while 180 meV are released for QcrC reduced by menaquinol. As *C. glutamicum bcc* complex has no cyt *c* substrate pool for driving the forward reaction, a larger redox potential difference close to PMF is advantageous. For *aa*$_3$ oxidase, 550 meV free energy are liberated from dioxygen reduction in mitochondria [62], whereas 700 meV are released when di-heme QcrC is injecting an electron. As a result, an excess of 150 meV free energy is available in *C. glutamicum aa*$_3$ oxidase to drive electron transfer and proton pumping. Thus, the association of *bcc* complex and *aa*$_3$ oxidase also appears to be energetically favorable for an efficient operation to pump protons in the presence of PMF.

4. Conclusion

We show that characteristic for *Actinobacteria* is the genetic composition for a respiratory supercomplex that is comprised of cyt *bcc* complex and cyt *aa*$_3$ oxidase. It is likely to be an obligatory supercomplex due to the lack of genes encoding alternative electron transfer partners. This *bcc-aa*$_3$ supercomplex is present in almost all actinobacterial species that are capable of aerobic metabolism. Based on characterization of the supercomplex from *C. glutamicum*, it combines a low potential *bcc* complex and a mixed potential *aa*$_3$ oxidase in defined spatial arrangement constrained by an indispensable short di-heme QcrC, thus facilitating energetically highly efficient coupled menaquinol oxidation and dioxygen reduction. Future studies need to elucidate the structural basis of redox tuning and the structural composition of the supercomplex. The actinobacterial supercomplex is of interest for improving efficiency of industrial production strains or for development of drugs against pathogens.

Transparency Document

The Transparency document associated with this article can be found, in the online version.

Acknowledgements

This work was supported by the German Research Foundation (CRC 746 to C.H., CRC 992 to C.H.) and the Excellence Initiative of the German Federal and State Governments (EXC 294 BIOSS to C.H.). P.H. is grateful to the Centre International de Recherche aux Frontière de la Chimie (icFRC, Strasbourg), the Agence National de la Recherche, CNRS and the University of Strasbourg. EPR facilities at EPR center of Aix-Marseille University received financial support from TGE RPE FR3443. We thank Dr. Christophe Wirth and Dr. Xenia Bogdanović for critical reading of the manuscript.

References

[1] B. Gao, R.S. Gupta, Phylogenetic framework and molecular signatures for the main clades of the phylum *Actinobacteria*, Microbiol. Mol. Biol. Rev. 76 (2012) 66–112, http://dx.doi.org/10.1128/MMBR.05011-11.
[2] G. Liu, K.F. Chater, G. Chandra, G. Niu, H. Tan, Molecular regulation of antibiotic biosynthesis in streptomyces, Microbiol. Mol. Biol. Rev. 77 (2013) 112–143, http://dx.doi.org/10.1128/MMBR.00054-12.
[3] L. Eggeling, M. Bott, Handbook of *Corynebacterium glutamicum*, CRC Press, Taylor & Francis Group, Boca Raton, Florida, USA, 2005.
[4] A.A. Vertès, M. Inui, H. Yukawa, The biotechnological potential of *Corynebacterium glutamicum*, from Umami to Chemurgy, Coryneacterium glutamicum, Springer, Berlin Heidelberg, Berlin, Heidelberg 2012, pp. 1–49, http://dx.doi.org/10.1007/978-3-642-29857-8_1.
[5] A. Burkovski, Diphtheria and its etiological agents, Corynebacterium diphtheriae, Springer, Netherlands 2013, pp. 1–14, http://dx.doi.org/10.1007/978-94-007-7624-1_1.
[6] A. Zumla, P. Nahid, S.T. Cole, Advances in the development of new tuberculosis drugs and treatment regimens, Nat. Rev. Drug Discov. 12 (2013) 388–404, http://dx.doi.org/10.1038/nrd4001.
[7] H. Schägger, K. Pfeiffer, Supercomplexes in the respiratory chains of yeast and mammalian mitochondria, EMBO J. 19 (2000) 1777–1783, http://dx.doi.org/10.1093/emboj/19.8.1777.
[8] E. Lapuente-Brun, R. Moreno-Loshuertos, R. Acín-Pérez, A. Latorre-Pellicer, C. Colás, E. Balsa, et al., Supercomplex assembly determines electron flux in the mitochondrial electron transport chain, Science 340 (2013) 1567–1570, http://dx.doi.org/10.1126/science.1230381.
[9] A. Niebisch, M. Bott, Molecular analysis of the cytochrome bc_1-aa_3 branch of the *Corynebacterium glutamicum* respiratory chain containing an unusual diheme cytochrome c_1, Arch. Microbiol. 175 (2001) 282–294.
[10] N. Sone, K. Nagata, H. Kojima, J. Tajima, Y. Kodera, T. Kanamaru, et al., A novel hydrophobic diheme *c*-type cytochrome. Purification from *Corynebacterium glutamicum* and analysis of the QcrCBA operon encoding three subunit proteins of a putative cytochrome reductase complex, Biochim. Biophys. Acta 1503 (2001) 279–290.
[11] M. Bott, A. Niebisch, The respiratory chain of *Corynebacterium glutamicum*, J. Biotechnol. 104 (2003) 129–153.
[12] Y. Kabashima, J.-I. Kishikawa, T. Kurokawa, J. Sakamoto, Correlation between proton translocation and growth: genetic analysis of the respiratory chain of *Corynebacterium glutamicum*, J. Biochem. 146 (2009) 845–855, http://dx.doi.org/10.1093/jb/mvp140.
[13] A. Niebisch, M. Bott, Purification of a cytochrome bc_1-aa_3 supercomplex with quinol oxidase activity from *Corynebacterium glutamicum*, J. Biol. Chem. 278 (2003) 4339–4346, http://dx.doi.org/10.1074/jbc.M210499200.
[14] K. Kusumoto, M. Sakiyama, J. Sakamoto, S. Noguchi, N. Sone, Menaquinol oxidase activity and primary structure of cytochrome *bd* from the amino-acid fermenting bacterium *Corynebacterium glutamicum*, Arch. Microbiol. 173 (2000) 390–397.
[15] A. Koch-Koerfges, N. Pfelzer, L. Platzen, M. Oldiges, M. Bott, Conversion of *Corynebacterium glutamicum* from an aerobic respiring to an aerobic fermenting bacterium by inactivation of the respiratory chain, Biochim. Biophys. Acta 1827 (2013) 699–708, http://dx.doi.org/10.1016/j.bbabio.2013.02.004.
[16] K. Pethe, P. Bifani, J. Jang, S. Kang, S. Park, S. Ahn, et al., Discovery of Q203, a potent clinical candidate for the treatment of tuberculosis, Nat. Med. 19 (2013) 1157–1160, http://dx.doi.org/10.1038/nm.3262.
[17] M.-S. Kim, J. Jang, N.B. Ab Rahman, K. Pethe, E.A. Berry, L.-S. Huang, Isolation and characterization of a hybrid respiratory supercomplex consisting of *Mycobacterium tuberculosis* cytochrome *bcc* and *Mycobacterium smegmatis* cytochrome aa_3, J. Biol. Chem. 290 (2015) 14350–14360, http://dx.doi.org/10.1074/jbc.M114.624312.
[18] M.D. Collins, D. Jones, Distribution of isoprenoid quinone structural types in bacteria and their taxonomic implication, Microbiol. Rev. 45 (1981) 316–354.
[19] K.I. Takamiya, P.L. Dutton, Ubiquinone in *Rhodopseudomonas sphaeroides*. Some thermodynamic properties, Biochim. Biophys. Acta 546 (1979) 1–16.
[20] R. Holländer, Correlation of the function of demethylmenaquinone in bacterial electron transport with its redox potential, FEBS Lett. 72 (1976) 98–100.
[21] M. Schütz, M. Brugna, E. Lebrun, F. Baymann, R. Huber, K.O. Stetter, et al., Early evolution of cytochrome *bc* complexes, J. Mol. Biol. 300 (2000) 663–675, http://dx.doi.org/10.1006/jmbi.2000.3915.
[22] B. Schoepp-Cothenet, C. Lieutaud, F. Baymann, A. Verméglio, T. Friedrich, D.M. Kramer, et al., Menaquinone as pool quinone in a purple bacterium, Proc. Natl. Acad. Sci. U. S. A. 106 (2009) 8549–8554, http://dx.doi.org/10.1073/pnas.0813173106.
[23] W.-C. Kao, C. Hunte, The molecular evolution of the Q_o motif, Genome Biol. Evol. 6 (2014) 1894–1910, http://dx.doi.org/10.1093/gbe/evu147.
[24] U.K. Laemmli, Cleavage of structural proteins during the assembly of the head of bacteriophage T4, Nature 227 (1970) 680–685.
[25] H. Schägger, 5 - Blue Native Electrophoresis, in: C. Hunte, G. von Jagow, H. Schägger (Eds.), Membrane Protein Purification and Crystallization (Second Edition), Academic Press, San Diego 2003, pp. 105–130.
[26] D. Moss, E. Nabedryk, J. Breton, W. Mäntele, Redox-linked conformational changes in proteins detected by a combination of infrared spectroscopy and protein electrochemistry. Evaluation of the technique with cytochrome *c*, Eur. J. Biochem. 187 (1990) 565–572.
[27] P. Hellwig, S. Grzybek, J. Behr, B. Ludwig, H. Michel, W. Mäntele, Electrochemical and ultraviolet/visible/infrared spectroscopic analysis of heme *a* and a_3 redox reactions in the cytochrome *c* oxidase from *Paracoccus denitrificans*: separation of heme *a* and a_3 contributions and assignment of vibrational modes, Biochemistry 38 (1999) 1685–1694, http://dx.doi.org/10.1021/bi982282.
[28] T. Wenz, P. Hellwig, F. MacMillan, B. Meunier, C. Hunte, Probing the role of E272 in quinol oxidation of mitochondrial complex III, Biochemistry 45 (2006) 9042–9052, http://dx.doi.org/10.1021/bi060280g.
[29] P. Hellwig, D. Scheide, S. Bungert, W. Mäntele, T. Friedrich, FT-IR spectroscopic characterization of NADH:ubiquinone oxidoreductase (complex I) from *Escherichia coli*: oxidation of FeS cluster N2 is coupled with the protonation of an aspartate or glutamate side chain, Biochemistry 39 (2000) 10884–10891, http://dx.doi.org/10.1021/bi000842a.
[30] P.L. Dutton, Oxidation-reduction potential dependence of the interaction of cytochromes, bacteriochlorophyll and carotenoids at 77 degrees K in chromatophores of *Chromatium* D and *Rhodopseudomonas gelatinosa*, Biochim. Biophys. Acta 226 (1971) 63–80.
[31] M. van Heel, G. Harauz, E.V. Orlova, R. Schmidt, M. Schatz, A new generation of the IMAGIC image processing system, J. Struct. Biol. 116 (1996) 17–24, http://dx.doi.org/10.1006/jsbi.1996.0004.
[32] S.R. Eddy, Accelerated profile HMM searches, PLoS Comput. Biol. 7 (2011) e1002195, http://dx.doi.org/10.1371/journal.pcbi.1002195.g006.
[33] M. Punta, P.C. Coggill, R.Y. Eberhardt, J. Mistry, J. Tate, C. Boursnell, et al., The Pfam protein families database, Nucleic Acids Res. 40 (2012) D290–D301, http://dx.doi.org/10.1093/nar/gkr1065.
[34] K.D. Pruitt, T. Tatusova, D.R. Maglott, NCBI reference sequences (RefSeq): a curated non-redundant sequence database of genomes, transcripts and proteins, Nucleic Acids Res. 35 (2007) D61–D65, http://dx.doi.org/10.1093/nar/gkl842.
[35] W. Li, A. Godzik, Cd-hit: a fast program for clustering and comparing large sets of protein or nucleotide sequences, Bioinformatics 22 (2006) 1658–1659, http://dx.doi.org/10.1093/bioinformatics/btl158.
[36] F. Sievers, A. Wilm, D. Dineen, T.J. Gibson, K. Karplus, W. Li, et al., Fast, scalable generation of high-quality protein multiple sequence alignments using Clustal Omega, Mol. Syst. Biol. 7 (2011) 539, http://dx.doi.org/10.1038/msb.2011.75.
[37] F. Ronquist, M. Teslenko, P. van der Mark, D.L. Ayres, A. Darling, S. Höhna, et al., MrBayes 3.2: efficient Bayesian phylogenetic inference and model choice across a large model space, Syst. Biol. 61 (2012) 539–542, http://dx.doi.org/10.1093/sysbio/sys029.
[38] S.F. Altschul, T.L. Madden, A.A. Schäffer, J. Zhang, Z. Zhang, W. Miller, et al., Gapped BLAST and PSI-BLAST: a new generation of protein database search programs, Nucleic Acids Res. 25 (1997) 3389–3402.
[39] A. Bernsel, H. Viklund, A. Hennerdal, A. Elofsson, TOPCONS: consensus prediction of membrane protein topology, Nucleic Acids Res. 37 (2009) W465–W468, http://dx.doi.org/10.1093/nar/gkp363.
[40] A. Krogh, B. Larsson, G. von Heijne, E.L. Sonnhammer, Predicting transmembrane protein topology with a hidden Markov model: application to complete genomes, J. Mol. Biol. 305 (2001) 567–580, http://dx.doi.org/10.1006/jmbi.2000.4315.
[41] S. Buschmann, E. Warkentin, H. Xie, J.D. Langer, U. Ermler, H. Michel, The structure of cbb_3 cytochrome oxidase provides insights into proton pumping, Science 329 (2010) 327–330, http://dx.doi.org/10.1126/science.1187303.
[42] A. Šali, T.L. Blundell, Comparative protein modelling by satisfaction of spatial restraints, J. Mol. Biol. 234 (1993) 779–815, http://dx.doi.org/10.1006/jmbi.1993.1626.
[43] T. Kleinschroth, M. Castellani, C.H. Trinh, N. Morgner, B. Brutschy, B. Ludwig, et al., X-ray structure of the dimeric cytochrome bc_1 complex from the soil bacterium *Paracoccus denitrificans* at 2.7-Å resolution, Biochim. Biophys. Acta 1807 (2011) 1606–1615, http://dx.doi.org/10.1016/j.bbabio.2011.09.017.
[44] M. Svensson-Ek, J. Abramson, G. Larsson, S. Törnroth, P. Brzezinski, S. Iwata, The X-ray crystal structures of wild-type and EQ(I-286) mutant cytochrome *c* oxidases from *Rhodobacter sphaeroides*, J. Mol. Biol. 321 (2002) 329–339, http://dx.doi.org/10.1016/S0022-2836(02)00619-8.
[45] R.J. Almassy, R.E. Dickerson, Pseudomonas cytochrome c_{551} at 2.0 Å resolution: enlargement of the cytochrome *c* family, Proc. Natl. Acad. Sci. U. S. A. 75 (1978) 2674–2678.

[46] R.E. Dickerson, Cytochrome *c* and the evolution of energy metabolism, Sci. Am. 242 (1980) 137–153.
[47] J. Heinemeyer, H.-P. Braun, E.J. Boekema, R. Kouril, A structural model of the cytochrome *c* reductase/oxidase supercomplex from yeast mitochondria, J. Biol. Chem. 282 (2007) 12240–12248, http://dx.doi.org/10.1074/jbc.M610545200.
[48] M.G. Finnegan, D.B. Knaff, H. Qin, K.A. Gray, F. Daldal, L. Yu, et al., Axial heme ligation in the cytochrome bc_1 complexes of mitochondrial and photosynthetic membranes. A near-infrared magnetic circular dichroism and electron paramagnetic resonance study, Biochim. Biophys. Acta 1274 (1996) 9–20.
[49] J.P. Hosler, M.P. Espe, Y. Zhen, G.T. Babcock, S. Ferguson-Miller, Analysis of site-directed mutants locates a non-redox-active metal near the active site of cytochrome *c* oxidase of *Rhodobacter sphaeroides*, Biochemistry 34 (1995) 7586–7592.
[50] G. von Jagow, T. Ohnishi, The chromone inhibitor stigmatellin – binding to the ubiquinol oxidation center at the C-side of the mitochondrial membrane, FEBS Lett. 185 (1985) 311–315.
[51] U. Liebl, A.W. Rutherford, W. Nitschke, Evidence for a unique Rieske iron-sulfur center in *Heliobacterium chlorum*, FEBS Lett. 261 (1990) 427–430.
[52] A. Riedel, A.W. Rutherford, G. Hauska, A. Müller, W. Nitschke, Chloroplast Rieske Center. EPR study on its spectral characteristics, relaxation and orientation properties, J. Biol. Chem. 266 (1991) 17838–17844.
[53] C. Hunte, S.R.N. Solmaz, H. Palsdottir, T. Wenz, A structural perspective on mechanism and function of the cytochrome bc_1 complex, Results Probl. Cell Differ. 45 (2008) 253–278, http://dx.doi.org/10.1007/400_2007_042.
[54] T. Tsukihara, H. Aoyama, E. Yamashita, T. Tomizaki, H. Yamaguchi, K. Shinzawa-Itoh, et al., The whole structure of the 13-subunit oxidized cytochrome *c* oxidase at 2.8 Å, Science 272 (1996) 1136–1144.
[55] C.J. Lentes, S.H. Mir, M. Boehm, C. Ganea, K. Fendler, C. Hunte, Molecular characterization of the Na^+/H^+-antiporter NhaA from *Salmonella* Typhimurium, PLoS One 9 (2014) e101575, http://dx.doi.org/10.1371/journal.pone.0101575.
[56] E.H.M.L. Heuberger, L.M. Veenhoff, R.H. Duurkens, R.H.E. Friesen, B. Poolman, Oligomeric state of membrane transport proteins analyzed with blue native electrophoresis and analytical ultracentrifugation, J. Mol. Biol. 317 (2002) 591–600, http://dx.doi.org/10.1006/jmbi.2002.5416.
[57] U. Liebl, S. Pezennec, A. Riedel, E. Kellner, W. Nitschke, The Rieske FeS center from the gram-positive bacterium PS3 and its interaction with the menaquinone pool studied by EPR, J. Biol. Chem. 267 (1992) 14068–14072.
[58] S. Duval, J.M. Santini, W. Nitschke, R. Hille, B. Schoepp-Cothenet, The small subunit AroB of arsenite oxidase: lessons on the [2Fe-2S] Rieske protein superfamily, J. Biol. Chem. 285 (2010) 20442–20451, http://dx.doi.org/10.1074/jbc.M110.113811.
[59] M. Ritter, O. Anderka, B. Ludwig, W. Mäntele, P. Hellwig, Electrochemical and FTIR spectroscopic characterization of the cytochrome bc_1 complex from *Paracoccus denitrificans*: evidence for protonation reactions coupled to quinone binding, Biochemistry 42 (2003) 12391–12399, http://dx.doi.org/10.1021/bi035103j.
[60] H. Yue, Y. Kang, H. Zhang, X. Gao, R.E. Blankenship, Expression and characterization of the diheme cytochrome *c* subunit of the cytochrome *bc* complex in *Heliobacterium modesticaldum*, Arch. Biochem. Biophys. 517 (2012) 131–137, http://dx.doi.org/10.1016/j.abb.2011.11.012.
[61] B.E. Schultz, S.I. Chan, Structures and proton-pumping strategies of mitochondrial respiratory enzymes, Annu. Rev. Biophys. Biomol. Struct. 30 (2001) 23–65, http://dx.doi.org/10.1146/annurev.biophys.30.1.23.
[62] P. Brzezinski, Redox-driven membrane-bound proton pumps, Trends Biochem. Sci. 29 (2004) 380–387, http://dx.doi.org/10.1016/j.tibs.2004.05.008.
[63] R.W. Hendler, H.V. Westerhoff, Redox interactions in cytochrome *c* oxidase: from the "neoclassical" toward "modern" models, Biophys. J. 63 (1992) 1586–1604, http://dx.doi.org/10.1016/S0006-3495(92)81748-4.
[64] C.C. Page, C.C. Moser, X. Chen, P.L. Dutton, Natural engineering principles of electron tunnelling in biological oxidation-reduction, Nature 402 (1999) 47–52, http://dx.doi.org/10.1038/46972.
[65] A. Marchler-Bauer, M.K. Derbyshire, N.R. Gonzales, S. Lu, F. Chitsaz, L.Y. Geer, et al., CDD: NCBI's conserved domain database, Nucleic Acids Res. 43 (2015) D222–D226, http://dx.doi.org/10.1093/nar/gku1221.
[66] R. Acín-Pérez, J.A. Enriquez, The function of the respiratory supercomplexes: the plasticity model, Biochim. Biophys. Acta 1837 (2014) 444–450, http://dx.doi.org/10.1016/j.bbabio.2013.12.009.
[67] M. Follmann, I. Ochrombel, R. Krämer, C. Trötschel, A. Poetsch, C. Rückert, et al., Functional genomics of pH homeostasis in *Corynebacterium glutamicum* revealed novel links between pH response, oxidative stress, iron homeostasis and methionine synthesis, BMC Genomics 10 (2009) 621, http://dx.doi.org/10.1186/1471-2164-10-621.